First-principles alloy theory in oxides

G Ceder†‡, A Van der Ven†, C Marianetti† and D Morgan†

† Department of Materials Science and Engineering, 77 Massachusetts Ave, Rm 13-5056, Cambridge, MA 02139, USA
‡ Center for Materials Science and Engineering, 77 Massachusetts Ave, Rm 13-5056, Cambridge, MA 02139, USA

Abstract. The physical mechanisms which may contribute to the energy and entropy of mixing in oxide systems are identified and discussed. Ionic size, magnetism and electrostatics can all contribute to the configurational energy dependence of transition-metal oxides. While the many sources of substitutional disorder make configurational entropy an essential contribution to the free energy of oxides, electronic and magnetic entropy may be of the same order of magnitude. This is illustrated with some first-principles results on $LiCoO_2$ and $LiMnO_2$.

1. Introduction

First-principles thermodynamics of crystalline materials is often referred to by the more general name of alloy theory, reflecting its historical focus on metallic mixtures. Accordingly, first-principles calculations have been applied to study a large number of binary metals [1–11], and even some ternaries [8, 12, 13]. An excellent overview of all the metallic systems investigated up to 1994 can be found in the review article by de Fontaine [14]. In the more recent decade much of the alloy theory formalism has been transferred to semiconductor alloys, with significant success [15].

Applications to oxides have been considerably more scarce, although the stimulus of high-temperature superconductivity led to some *ab initio* alloy work on the phase diagram of $Y_2Ba_2Cu_3O_{7-\delta}$ [16, 17] in the early 1990s. Perovskites with mixed B sites have also received attention because of their technological importance as ferroelectrics and dielectrics [18–22].

In this paper we identify the differences and similarities between alloy theory in oxides and metals. The varying degrees of electron localization possible in oxides poses significant challenges to a proper description of the entropy and energy as will be illustrated with examples from Li_xCoO_2 and $LiMnO_2$.

2. Sources of configurational entropy in oxides

In metallic systems, configurational entropy is the key to reproducing the correct phase diagram topology of alloys. Similarly, it is an essential part of a correct description of oxide thermodynamics. There are several sources of substitutional disorder in oxides which may contribute to the configurational entropy. As in metals, multiple cations or anions can share a common sublattice. This is, for example, the case in $Ba(Zn_{1/3}Nb_{2/3})O_3$ where Zn and Nb ions are distributed over the cubic lattice of B-sites in the perovskite structure (figure 1(a)) [21].

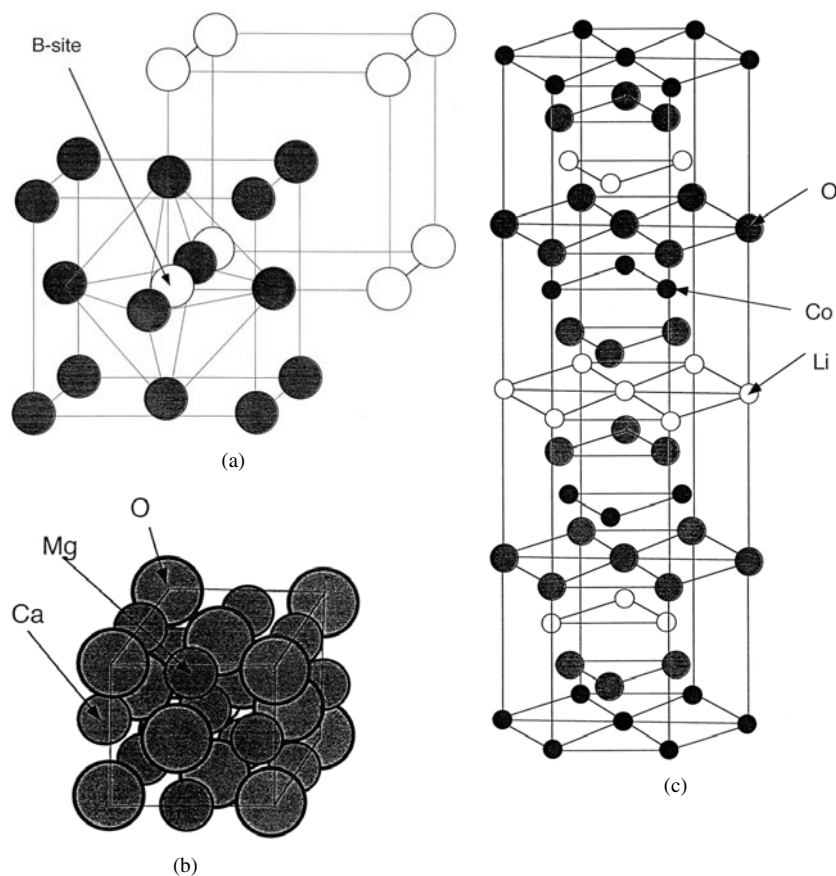**Figure 1.** (a) Cubic perovskite unit cell. The B sites (white circles) form a simple cubic lattice. (b) In $Ca_xMg_{1-x}O$ rocksalts the Ca and Mg ions mix on the fcc lattice of octahedral interstitials (c) $LiCoO_2$ is a rocksalt with Li and Co ions ordered in alternating planes of octahedral sites along the rocksalt (111) direction. Lithium can be removed electrochemically leading to order–disorder transitions between lithium and vacancies.

In $Ca_xMg_{1-x}O$ the cations share a common fcc lattice, formed by the octahedral interstices of the close-packed oxygen framework (figure 1(b)) [23]. While this type of cationic disorder is quite similar to that in binary metals, the filled anion array in oxides plays a key role in the interaction between the cation sites.

Because many oxides can be seen as close-packed anion arrays with metal interstitials, many structures are at least mechanically stable against removal of a substantial fraction of metal ions. This can lead to configurational disorder between filled and vacant sites. Li_xCoO_2 (figure 1(c)) is an extreme example of this type of substitutional disorder as x (the amount of Li per formula unit) can be varied between 0 and 1 with little or no variation of the host structure. Over this composition range the Li ions go through several order–disorder reactions with the vacancies [24–27]

Due to their structural role the concentration of anion vacancies is usually not as large as for cations and often requires the presence of large cations such as Ba^{2+} or Pb^{2+} that reside in the oxygen framework. Hence, $YBa_2Cu_3O_{7-\delta}$ can have oxygen-vacancy order–disorder transitions [16, 17] as does $Ba_2In_2O_{6-\delta}$ [28, 29].

One should keep in mind that the types of disorder mentioned above can occur simultaneously on different sublattices in one system. For example, in pyrochlores of composition $A_2B_2O_7$ the A and B cations order on the sites of an fcc-like sublattice while oxygen-vacancy ordering takes place on the tetrahedral interstitials of this lattice [30–32]. Partial disorder on these sublattices is intricately linked [33]. Similarly, disorder on the transition metal cation sublattice of materials such as $Li_x(Ni, Co)O_2$ is found to depress the ordering tendency of Li and vacancies [34]. Such coupled order–disorder problems are common in oxides as they often arise from the charge compensation mechanism that couples the off-stoichiometry on different sublattices. For example, when ZrO_2 is alloyed with CaO, the mixing of Ca onto the Zr sublattice is accompanied by the creation of oxygen vacancies on the anion sublattice. The configurational state of each of these sublattices can be strongly coupled, even in a fully-disordered state.

Coupling between disorder on various sublattices can be dominated by symmetry, coupling interactions or correlated fluctuations [33].

3. Configurational expansions

The methods to describe configurational disorder and its effect on a free energy are now well developed. We review them here only briefly, with some attention paid to the coupling of disorder between various sublattices. The approach consists of coarse graining the faster degrees of freedom (such as vibrational and electronic) [35] until only substitutional degrees of freedom remain in the partition function. The free energy corresponding to such a partition function can then be calculated by standard methods for lattice models. The Hamiltonian of the effective lattice model is obtained with a cluster expansion [36]. The cluster expansion method is described in several excellent reviews [14, 15]. Basically, it characterizes the configurational state with occupation variables σ_i for each lattice site i (e.g. σ_i is ± 1 depending on occupation of site i by species A or B, where one of these can be a vacancy). The energy is then expanded in polynomials of the occupation variables. The polynomials φ_α correspond to products of occupation variables within a cluster of lattice sites α,

$$\varphi_\alpha = \prod_{i \in \alpha} \sigma_i \tag{1}$$

and are referred to as cluster functions. These clusters are, for example, pairs, triplets, quadruplets of sites, etc. Their corresponding functions form a complete and orthonormal basis. Any property of a configuration, such as the energy, volume, etc can, therefore, be expressed as a linear combination of the polynomials φ_α. A cluster expansion of the configurational energy, for example, takes the form

$$E = V_0 + \sum_\alpha V_\alpha \cdot \varphi_\alpha \tag{2}$$

where the summation extends over all clusters α, and V_0 and the V_α are constant expansion coefficients. The expansion coefficients for the energy are generally called effective cluster interactions (ECIs).

Typically, the values of the ECIs are calculated from first principles energy models by fitting the expansion to the energy of a series of ordered configurations described by small supercells. The fit to the first-principles energies can be performed with either a least-squares procedure or a more elaborate method based on linear programming techniques [1].

The cluster expansion can be extended to systems in which multiple sublattices contain substitutional disorder [33]. An appropriate basis for the system as a whole can be constructed from the cluster functions describing the disorder on each individual sublattice. If φ_α and θ_β

are respectively the cluster functions describing the binary disorder on two separate sublattices, the new basis function

$$\psi_{\alpha\beta} = \varphi_\alpha \theta_\beta \tag{3}$$

can describe the state of the total system. This basis offers an unbiased description of the configuration of all ions and does not rely on any simplifying assumptions often used in modelling defects in oxides (such as the association between vacancies and dopant cations, etc).

4. Factors that contribute to the effective cluster interactions

In metallic systems, the ECIs are largely defined by direct metal–metal orbital overlap. We discuss below the physical phenomena that determine the ECI in oxides as they can be considerably different from those in metals.

Ionic size effects are often the most dominant contribution to the effective interactions in oxides. Insertion of a large cation into the interstitial of a close-packed oxygen framework will displace the oxygen ions around it, thereby changing the energy required to insert an ion at a neighbouring site. Note that the relaxation of oxygen ions around an inserted cation is not necessarily outwards, since it is a competition between an inward relaxation (due to the electrostatic attraction between the oxygen and cation) and the outward relaxation due to steric effects. In closed-shell oxides, such as MgO or CaO, indirect interaction through oxygen displacements is practically the only contribution to the ECIs, and empirical energy models with no direct cation–cation interaction can qualitatively reproduce the experimental phase diagram [23]. Many cation ordered structures can be explained on the basis of size alone.

Covalent interaction through direct overlap of atomic wavefunctions, one of the main factors which determines the ordering or phase separation in metals [37, 38], has often a small effect in oxides. This is due to the rather contracted nature of orbitals (e.g. in 3d transition-metal oxides) or the complete absence of any valence electrons (e.g. closed-shell oxides such as MgO).

Electrostatic interactions are obviously a key contribution to the effective interactions between differently charged cations. In some cases, the electrostatic interactions dominate over all others and the stable structure can be obtained by simply minimizing the Madelung energy of a distribution of ions over fixed lattice sites. Examples include the perovskites $Ba(Mg_{1/3}Ta_{2/3})O_3$ and $Ba(Zn_{1/3}Ta_{2/3})O_3$ [20, 21, 39–41] in which the B cations are ordered in a 1:2 repeat period along the $\langle 111 \rangle$ cubic perovskite direction. Several studies [20, 42] have indicated that this configuration is the one with the lowest electrostatic energy for a system with composition $(1/3, 2/3)$ on a cubic lattice.

In other systems relaxation effects and electrostatics compete for different ground states [43]. ABO_2 ordered rocksalts form the $LiScO_2$ structure which is the electrostatic ground state, when the A and B cations are similar in size, while the α-$NaFeO_2$ structure is formed for equiatomic mixtures of large and small cations (e.g. $LiCoO_2$ or $LiAlO_2$ [43]). The latter structure is preferred for systems with very different cation size because its symmetry allows for independent anion relaxations around each type of cation.

Electrostatic interactions can be screened considerably by the high polarizability of the oxygen atoms or by the presence of transition metal ions with variable valence. Figure 2 shows the change in electron density in Li_xCoO_2 when two Li ions are inserted into CoO_2. The plane shown is defined by the oxygen, cobalt and lithium positions in the unit cell. Although Li is ionized to +1, a large screening electron accumulation is present on the oxygen orbitals
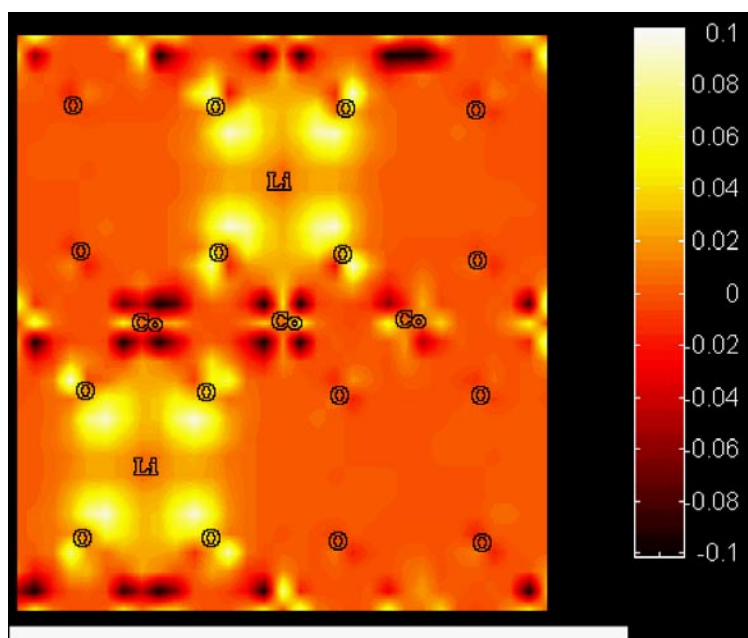
Figure 2. Electron density change when two Li ions are inserted into CoO_2. Yellow means electron gain while black indicates a decrease in electron density.

surrounding the Li ions. This effect can reduce the bare Coulombic interaction between neighbouring Li ions by a factor of 40†. As a result Li ordering barely persists above room temperature.

Besides size, electrostatic and covalent effects, *electron-lattice coupling* and *magnetism* can play a significant role in oxides. Because of the localized nature of electron orbitals in many oxides, partially-filled degenerate states can easily lead to spontaneous symmetry breaking of the environment around the cation. Peierls or Jahn–Teller distortions are therefore quite prevalent in transition metal oxides [44]. For example, in $LiMnO_2$, oxygen octahedra around Mn^{3+} are significantly Jahn–Teller distorted in order to break the degeneracy of the two e_g orbitals (figure 3). The degeneracy is broken by lengthening one of the octahedral axes, lowering the energy of the d_{z^2} orbital which lies along this axis. The energy is lowered because the e_g (d_{z^2}) orbital is antibonding and therefore becomes lower in energy with increasing ion separation. In $LiMnO_2$ the difference between the short and long bonds of the MnO_6 octahedron can be as much as 20%, making effectively for an 'elliptical' Mn ion [45].

Such local environment changes can make for 'hidden' configurational problems. For example, when Li is partially removed from $LiMnO_2$, configurational disorder not only occurs on the Li-vacancy sublattice but also on the Mn sublattice due to the creation of Jahn–Teller (Mn^{3+}) and non-Jahn–Teller (Mn^{4+}) ions. Such electronically coupled configurational problems pose an interesting challenge to *ab initio* alloy theory.

Magnetism is expected to be more important in oxides than it is in metals due to the large magnetic moments that are often found on transition metal cations in an oxide. In addition, the localized nature and valence dependence of the moments can couple them directly to

† This can be seen from comparing the effective interaction, calculated in [25] with the bare electrostatic potential.
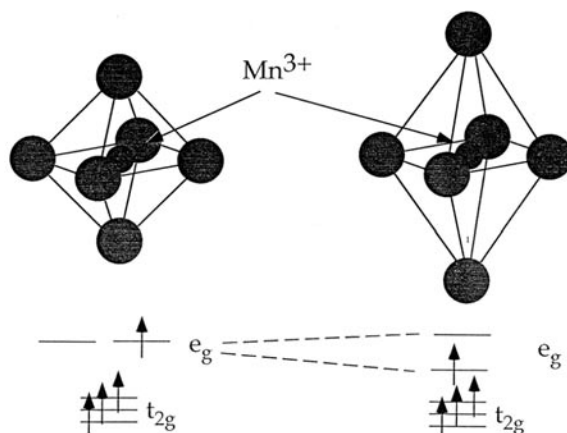
Figure 3. The Jahn–Teller distortion of an octahedron around Mn^{3+} splits the degenerate e_g levels.
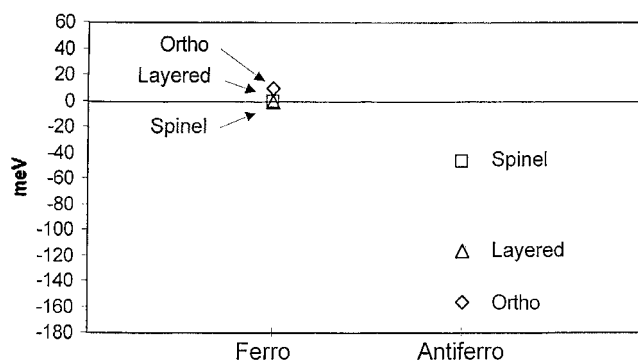

Figure 4. Energy of three different lithium manganese orderings in rocksalts with ferromagnetic and antiferromagnetic spin polarization.

ionic configuration changes on other sublattices. Figure 4 shows the relative stability of three different orderings of Li and Mn over the octahedral sites of the rocksalt lattice in $LiMnO_2$ as calculated with an ultra-soft pseudopotential method [45]. Note that magnetism has a substantial effect on the energy differences between these structures. Ferromagnetic and antiferromagnetic spin ordering even leads to a different ground state. Such interplay between magnetism and structural stability can be used to tailor the relative stability of these structures with compositional changes [46].

Magnetism can also cause several metastable configurations to appear for a particular ionic arrangement [47]. Figure 5 shows the energy versus volume for a lithiated $Li_2Mn_2O_4$ spinel for different spin and symmetry states. The lowest energy is obtained for a Jahn–Teller distorted structure (triangles in figure 5) in which Mn is high spin ($t_{2g}^3 e_g^1$ electronic configuration). The Jahn–Teller distortion makes the otherwise cubic spinel unit cell tetragonal and splits the e_g levels. At significantly lower volume the same structure, but with partially low-spin Mn, has another local minimum (diamond symbols). This minimum corresponds to Mn^{3+} in configuration $t_{2g}^4 e_g^0$ with an electron-only moment of $2\mu_B$. Because of the reduced spin on the Mn ion, the symmetry of this spinel is cubic. Also shown (circles) is the energy versus volume for a spinel with cubic symmetry (thereby not allowing for the Jahn–Teller
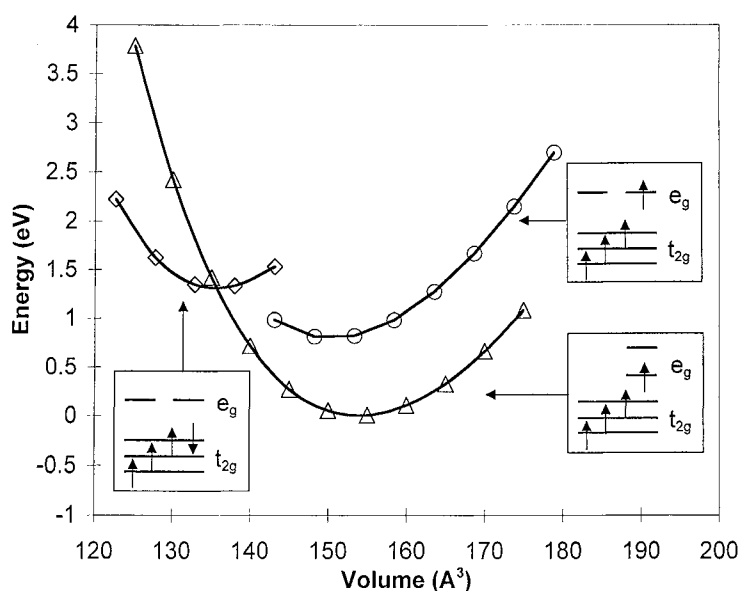
Figure 5. Energy versus volume for different electronic states of $LiMnO_2$.

distortion) and high-spin Mn^{3+}. All three structures are local minima in the density functional theory equation of state. Care should therefore be exercised to obtain the correct electronic and magnetic ground states when calculating energy differences or phase diagrams for these materials. To our knowledge, such magnetism-induced metastability has never been observed before in density functional theory calculations.

5. Non-configurational entropy

While application of lattice model statistical mechanics, such as the cluster variation method [48] or Monte Carlo simulation, to the cluster expansion can determine the configurational entropy explicitly, the entropy arising from other excitations has to be implicitly included in the values of ECIs. These additional entropy contributions make the ECIs temperature dependent [35]. In metallic alloys both vibrational [49–51] and electronic entropy [52] have been included in this way. Oxides may produce additional sources of entropy which cannot easily be dealt with. When identical ions with different valence are present (such as Mn^{3+} and Mn^{4+} or Cu^{1+} and Cu^{2+}) a configurational-like electronic entropy term should be considered [53, 54]. While an ideal-solution term can be easily added to account for the configurational disorder of different valence states, problems arise when this distribution is coupled to the configurations of ions on another sublattice (e.g. Li vacancy and Mn^{3+}/Mn^{4+} ordering in Li_xMnO_2). Since the concentration of Mn^{3+} is equal to the lithium concentration, total decoupling of the Mn and Li sublattice would generate an entropy of $-2k_B[x \ln x + (1-x) \ln(1-x)]$ (assuming fully disordered states on both sublattices). However, localization of the Mn^{3+} ions near Li (as opposed to vacancies) would strongly reduce this entropy, and in the limit of fully-coupled configurational states the entropy would be only $-k_B[x \ln x + (1-x) \ln(1-x)]$. The uncertainty in the configurational entropy associated with the electronic coupling between the two sublattices is therefore of the same order of magnitude

as the total entropy. The localized-charge entropy can further be reduced by *delocalization* (bringing the entropy towards the metallic limit) or by charge *ordering* (bringing it towards zero) [55, 56]. Calculation of the electronic entropy between the localized and delocalized limit will require the development of electronic structure methods that go beyond the local density approximation.

Besides entropy associated with the 'localization' of electrons, entropy can arise from the different orientations of symmetry breaking transitions, such as Jahn–Teller distortions, or ordering of the magnetic moments.

6. The $Li_x CoO_2$ phase diagram: failure of density functional theory around a metal–insulator transition

$Li_x CoO_2$ is an important material for applications in rechargeable lithium batteries as it reversibly intercalates lithium ions with little change to the CoO_2 host framework. In the discharge cycle of a Li battery, Li is absorbed by the host material. Upon charging this process is reversed. While laboratory experiments have shown reversible lithium intercalation between $x = 0$ and $x = 1$ on $Li_x CoO_2$ [57], cycling in commercial batteries is limited to the range $0 < x < 0.5$.

Figure 1(c) shows the $LiCoO_2$ structure which consists of close-packed oxygen layers stacked in ABC sequence with Li and Co occupying alternating planes of octahedral interstices. Since the octahedral interstices of an ABC stacked oxygen framework form an fcc lattice, a one-to-one correspondence exists between the possible Li–Co distributions and the ground states of fcc lattice models. The specific ordering of $LiCoO_2$ is $L1_1$ (or CuPt prototype in alloys). As Li is extracted from $LiCoO_2$, Li-vacancy ordering can occur. Figure 6(a) shows the calculated phase diagram for this material as a function of lithium content. An experimental compilation of results is shown in figure 6(b). For $x > 0.25$ the host material shown in figure 1(c) is stable. For $x < 0.25$ minor modifications in the oxygen framework are predicted to occur, necessitating the use of cluster expansions on different lattices. One should keep in mind that the phase diagram of figure 6(a) indicates the most stable states in the layered structures or variants thereof, and it cannot be excluded that other host structures are more stable. Finding the most stable host structures among the infinite number of possibilities is still an unsolved problem in first-principles materials theory. More details on this specific calculation can be found in [25]. In general, there is quite good agreement between the calculated and experimental results. The ordered Li-vacancy configuration predicted to occur at $x = 0.5$ is the same as the one put forward on the basis of XRD data [26]. In addition, the H1-3 phase, a structure in which Li ions occupy only every other possible plane, is consistent with the observed changes in XRD patterns around that composition [58]. However, one significant discrepancy exists between the calculated and experimental information. Experimentally, two phases with distinct Li composition but identical symmetry are predicted to occur between $x = 0.75$ and $x = 0.95$. In the calculation no such two-phase region can be observed. This failure of *ab initio* alloy theory to reproduce this phase transition is consistent with the recent understanding that it cloaks a metal–insulator transition [25, 59]. While $LiCoO_2$ is a semiconductor, removal of Li introduces localized holes in the Co t_{2g} valence band. It is expected that at a critical concentration these holes overlap and the material becomes metallic. The view of this transition as a metal–insulator transition has recently been reinforced by conductivity and NMR measurements as a function of Li content [59]. Density functional theory, which was the basis for the calculated diagram of figure 6(a), cannot be expected to capture the subtle energetic and entropic effects associated with such an electronic transition.
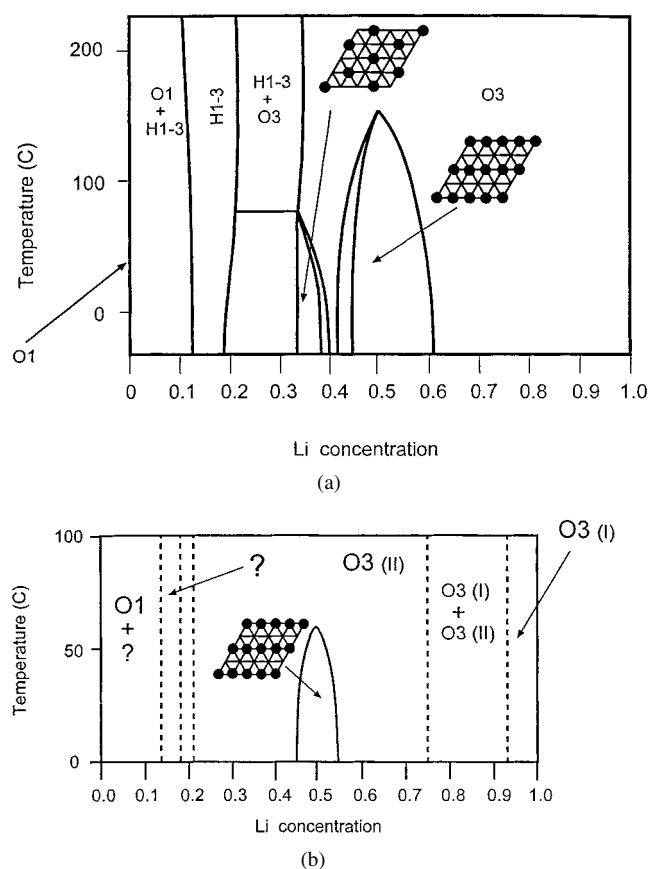
Figure 6. (a) Calculated Li_xCoO_2 phase diagram. (b) Experimentally compiled Li_xCoO_2 phase diagram.

The calculated phase diagram in figure 6(a) shows the strong screening effect of the Li–Li interaction. The phase diagram is highly asymmetric with respect to lithium concentration. This can be understood from the charge compensation mechanism in these structures. The electrostatic interaction between the positively charged Li^+ ions in $LiCoO_2$ is strongly screened by the large and polarizable electron density on the oxygen ions. As Li is removed from $LiCoO_2$, charge neutrality requires the removal of electron density from the CoO_2 framework. Since this electron density is largely taken from the oxygen ions [60, 61], Li removal reduces the screening power of the oxygens, thereby increasing the effective Li–Li interaction.

7. Conclusion

Although alloy theory has been successful in predicting and explaining the phase diagrams of binary metals, oxides present a new series of challenges for this field. The strong coupling between electronic, magnetic, positional and configurational degrees of freedom may necessitate the development of a temperature-dependent electronic theory which can describe the continuous transition between the localized and delocalized states that can occur in oxides.

Acknowledgments

References

[1] Garbulsky G D and Ceder G 1995 *Phys. Rev.* B **51** 67–72
[2] Ceder G, de Fontaine D, Dreysse H, Nicholson D M, Stocks G M and Gyorffy B L 1990 *Acta Metall. Mater.* **38** 2299–308
[3] Asta M, de Fontaine D, Van Schilfgaarde M and Sluiter M 1992 *Phys. Rev.* B **46** 5055–72
[4] Asta M, McCormack R and de Fontaine D 1993 *Phys. Rev.* B **48** 748–66
[5] Sluiter M, Turchi P E A, Pinski F J and Stocks G M 1992 *J. Phase Equilibria* **13** 605–11
[6] Sluiter M, Turchi P, Zezhong F and de Fontaine D 1988 *Phys. Rev. Lett.* **60** 716
[7] Turchi P E A, Sluiter M, Pinski F J, Johnson D D, Nicholson D M, Stocks G M and Staunton J B 1991 *Phys. Rev. Lett.* **67** 1779–82
[8] Wolverton C M 1993 *PhD Thesis* University of California at Berkeley
[9] Wolverton C, Ceder G, de Fontaine D and Dreyssé H 1993 *Phys. Rev.* B **48** 726–47
[10] Burton B P, Osburn J E and Pasturel A 1992 *Phys. Rev.* B **45** 7677–83
[11] Sanchez J M, Stark J P and Moruzzi V L 1991 *Phys. Rev.* B **44** 5411
[12] McCormack R, de Fontaine D, Wolverton C and Ceder G 1995 *Phys. Rev.* B **51** 15 808–22
[13] de Rooy A, Van Royen E W, Bronsveld P M and de Hosson J T M 1980 *Acta Metall.* **28** 1339–47
[14] de Fontaine D 1994 *Solid State Physics* vol 47, ed H Ehrenreich and D Turnbull (New York: Academic) pp 33–176
[15] Zunger A 1994 *Statics and Dynamics of Alloy Phase Transformations* ed P E A Turchi and A Gonis (New York: Plenum) pp 361–419
[16] Ceder G, Asta M, Carter W C, Sluiter M, Mann M E, Kraitchman M and de Fontaine D 1990 *Phys. Rev.* B **41** 8698–701
[17] Ceder G 1994 *Molec. Simul.* **12** 141–53
[18] Burton B P and Cohen R E 1995 *Phys. Rev.* B **52** 792–7
[19] Burton B P 1999 *Phys. Rev.* B **59** 6087–91
[20] Takahashi T, Wu E, Van der Ven A and Ceder G 1999 *Japan. J. Appl. Phys.* at press
[21] Takahashi T, Wu E and Ceder G 1999 *J. Mater. Res.* submitted
[22] Bellaiche L, Padila J and Vanderbilt D 1999 *Phys. Rev.* B **59** 1834–9
[23] Tepesch P D, Kohan A F, Garbulsky G D, Ceder G, Coley C, Stokes H T, Boyer L L, Mehl M J, Burton B, Cho K and Joannopoulos J 1996 *J. Am. Ceram. Soc.* **79** 2033–40
[24] Ceder G and Van der Ven A 1999 *Electrochimica Acta* **45** 131–50
[25] Van der Ven A, Aydinol M K, Ceder G, Kresse G and Hafner J 1998 *Phys. Rev.* B **58** 2975–87
[26] Reimers J N and Dahn J R 1992 *J. Electrochem. Soc.* **139** 2091–7
[27] Wolverton C and Zunger A 1998 *Phys. Rev. Lett.* **81** 606–9
[28] Goodenough J B, Ruiz-Diaz J E and Zhen Y S 1990 *Solid State Ion.* **44** 21–31
[29] Prasanna T R S and Navrotsky A 1993 *J. Mater. Res.* **8** 1484–6
[30] Haile S M and Wuensch B J P E 1990 *Neutron Scattering for Materials Science (Mater. Res. Soc. Symp. Proc., vol 166)* ed S M Shapiro, S C Moss and J D Jorgensens pp 81–6
[31] Tepesch P D and Ceder G 1997 *Computational Modeling of Materials and Processing (Ceramic Transactions, vol. 69)* ed J H Simmons, E R Fuller, A L Dragoo and E J Garboczis pp 123–8
[32] Ceder G, Kohan A F, Aydinol M K, Tepesch P D and Van der Ven A 1998 *J. Am. Ceram. Soc.* **81** 517–25
[33] Tepesch P D, Garbulsky G D and Ceder G 1995 *Phys. Rev. Lett.* **74** 2272–5
[34] Reimers J N, Dahn J R and Von Sacken U 1993 *J. Electrochem. Soc.* **140** 2752–4
[35] Ceder G 1993 *Comput. Mater. Sci.* **1** 144–50
[36] Sanchez J M, Ducastelle F and Gratias D 1984 *Physica* A **128** 334–50
[37] Ducastelle F 1991 Cohesion and structure *Order and Phase Stability in Alloys* vol 3, ed F R de Boer and D G Pettifor (Amsterdam: North-Holland)
[38] Pettifor D G 1978 *Solid State Commun.* **28** 621–3

[39] Burton B P and Cohen R E 1994 *Third Williamsburg Workshop on First Principles Calculations for Ferroelectrics* vol 164, pp 201–12

[40] McCormack R and Burton B P 1996 *Symp. on Solid-State Chemistry of Inorganic Materials* ed P K Davies, A J Jacobson, C C Torardi and T A Vanderahs pp 449–54

[41] Burton B P, McCormack R P, Toby B H and Goo E K 1996 *Fourth Williamsburg Workshop on First Principles Calculations for Ferroelectrics* vol 194, pp 187–206

[42] Bellaiche L V 1998 *Phys. Rev. Lett.* **81** 1318–21

[43] Wu E J, Tepesch P D and Ceder G 1998 *Phil. Mag.* B **77** 1039–47

[44] Burdett J K 1995 *Chemical Bonding in Solids* (New York: Oxford University Press)

[45] Mishra S K and Ceder G 1999 *Phys. Rev.* B **59** 6120–30

[46] Ceder G and Mishra S K 1999 *Electrochem. Solid State Lett.* **2** 550–2

[47] Van der Ven A, Marianetti C, Morgan D and Ceder G 1999 *Solid State Ion.* at press

[48] Kikuchi R 1951 *Phys. Rev.* **81** 988–1003

[49] Van de Walle A and Ceder G 2000 *Phys. Rev.* B **61** 5972–8

[50] Van de Walle A, Ceder G and Waghmar U 1998 *Phys. Rev. Lett.* **80** 4911–14

[51] Ozolins V, Wolverton C and Zunger A 1998 *Phys. Rev.* B **58** R5897–900

[52] Wolverton C and Zunger A 1995 *Phys. Rev.* B **52** 8813–28

[53] Schleger P, Hardy W N and Casalta H 1994 *Phys. Rev.* B **49** 514–23

[54] Tetot R, Pagot V and Picard C 1999 *Phys. Rev.* B **59** 14 748–52

[55] Ahn K H and Millis A J 1998 *Phys. Rev.* B **58** 3697–703

[56] Rodríguez-Carvajal J, Rousse G, Masquelier C and Hervieu M 1998 *Phys. Rev. Lett.* **81** 4660–3

[57] Amatucci G G, Tarascon J M and Klein L C 1996 *J. Electrochem. Soc.* **143** 1114–23

[58] Van der Ven A, Aydinol M K and Ceder G 1998 *J. Electrochem. Soc.* **145** 2149–55

[59] Menetrier M, Saadoune I, Levasseur S and Delmas C 1999 *J. Mater. Chem.* **9** 1135–40

[60] Ceder G, Aydinol M K and Kohan A F 1997 *Comput. Mater. Sci.* **8** 161–9

[61] Ceder G, Chiang Y-M, Sadoway D R, Aydinol M K, Jang Y-I and Huang B 1998 *Nature* **392** 694–6